Journal of the Korean Society of Marine Environment & Safety
Research Paper
Vol. 22, No. 6, pp. 615-624, October 31, 2016, ISSN 1229-3431(Print) / ISSN 2287-3341(Online) http://dx.doi.org/10.7837/kosomes.2016.22.6.615

A Numerical Simulation of Hydrodynamic Interactions Between Two Moored Barges with Regular Waves

Sang-Do Lee* · Byung-Deug Bae** · Dae-Hae Kim***†

* Graduate School of Korea Maritime and Ocean University, Busan 49112, Korea
** Division of Ship Navigation, Korea Maritime and Ocean University, Busan 49112, Korea
*** Korea e-Navi Information Technology Co. LTd., Busan, Korea

규칙파 중 계류된 두 바지선의 유체역학적 상호작용에 관한 수치시뮬레이션

이상도* · 배병덕** · 김대해***†

* 한국해양대학교 대학원, ** 한국해양대학교 선박운항과, *** 한국이네비정보기술(주)

Abstract : *In this study, two rectangular barges in close proximity were simulated to analyze the characteristics of motion responses due to hydrodynamic interactions. Using a numerical solution from DNV-GL SESAM, coupled stiffness matrix terms for these same FEM models were added to the multiple body modes in the surge direction. Potential theory was used to calculate the first order radiation and diffraction effects on the simulated barge models. In the results, the sheltering effect of the barges was not shown at 1.3 rad/s with hull separation of 20 m in transverse waves. The separation effect between the barges was more clear with longitudinal waves and a shallow water depth. However, sway forces were influenced by hull separation with transverse waves. The peaks for sway and heave motion and sway force occurred at higher frequencies as hull separation narrowed with longitudinal and transverse waves. Given a depth of 10 m, the sway motion on the lee side of a coupled barge made a significant difference in the range of 0.2-0.8 rad/s with transverse and oblique waves. Also, the peaks for sway force were situated at lower frequencies, even when incident waves changed.*

Key Words : *Hydrodynamic interactions, Sheltering effect, Hull separation, Wave direction, Lee side barge*

요 약 : 본 연구는 해상에서 근접하여 계류된 직사각형 박스 형상의 두 바지선을 대상으로 유체역학적 상호작용으로 인한 선체운동 응답특성을 분석하기 위하여 수치시뮬레이션을 실시하였다. 이 수치시뮬레이션 실험에서는 DNV-GL의 SESAM 수치해석솔루션을 사용하여 결합된 강성 메트릭스항(coupled stiffness matrix terms)을 다중물체 모드(multiple body modes)의 surge 방향에 추가하였고, 실험에 적용한 바지선 모델의 1차 방사 및 산란 영향을 계산하기 위하여 퍼텐셜 이론을 적용하였다. 실험 결과, 두 바지선의 횡간격 20 m, 횡파 실험조건 경우에 1.3 rad/s에서 실험선의 피난효과(sheltering effect)가 나타나지 않았다. 실험 모델 상호간 횡간격의 영향은 종파와 천수역 실험 조건에서 분명하게 나타났지만, sway force는 횡파일 경우에 두 실험 모델선과의 접근거리 간격에 영향을 받았다. 실험모델의 횡간격이 좁아지면 종파와 사파의 경우에 sway, heave 운동과 sway force의 피크는 높은 주파수대로 이동하였다. 수심이 10 m일 때 풍하측 바지선의 sway 운동은 횡파와 사파의 경우에 0.2-0.8 rad/s 주파수대에서 큰 차이를 보였으며, 입사파의 방향이 달라져도 sway force의 피크는 보다 낮은 주파수대에서 나타났다.

핵심용어 : 유체역학적 상호작용, 피난효과, 횡간격, 파향, 풍하측 바지선

* First author : oksangdo@naver.com
† Corresponding Author : kim_daehae@naver.com

1. Introduction

When considering the safe navigation and cargo operation between two adjacent ships, special attention should be paid to the hydrodynamic interaction that produces the unfavorable motion and forces closely related to the collision. For decades, many researchers have been devoted much effort to investigating this topics.

Bucher et al. (2001) developed a numerical multiple body simulation model during side by side off-loading operation. Hong et al. (2005) investigated the motion and drift forces of moored multiple vessels arranged side by side using a higher-order boundary element method. Choi and Hong (2002) also used the same method to calculate the motions and drift forces of rectangular barges in parallel and tandem arrangements. Ali and Inoue (2005) used 3D source-sink method to determine the hydrodynamic coefficients and exciting forces of two rectangular barges floated without moorings. Fournier et al. (2006) focused on the resonance problem of the wave elevation between two side by side ships. Kim and Kim (2008) adopted 3D Rankine panel method to calculate the motions of adjacent multiple bodies in time domain. Bunnik et al. (2009) computed the hydrodynamic interaction of side by side moored LNG carriers using a damping lid method to suppress wave elevation. Clauss et al. (2013) investigated the gap effects of typical barge and carrier in parallel arrangement. Recently, Pessoa et al. (2015) investigated a numerical study of the coupled dynamic responses of side by side LNG floating systems using a higher order boundary element method.

In this paper, numerical simulations are conducted on the two adjacent rectangular barges to investigate the characteristics of motion responses due to hydrodynamic interactions. We compared the results of coupled barges with single barge calculation. Several factors such as wave direction, hull separation and water depth are considered. Since the barges are restrained by moorings in x-translation, surge motion is bigger than other motions because of the spring forces in x-translation. For a floating unit the natural periods of motions are key features and ocean waves contain 1st harmonic wave energy in the period range of 5-25s (DNV, 2010a).

2. Background Theory

2.1 Multi-body modelling

The hydrodynamic interaction is computed from the potential theory as applied for a single structure. The coordinate systems of multi-body problems are different from those of a single-body analysis. The coordinate systems are defined as follows (DNV, 2010b).

1) The global coordinate system (X_{glo}, Y_{glo}, Z_{glo}) with its origin at still water level and the z-axis normal to the still level and the positive z-axis pointing upwards.

2) The individual body coordinate system (X_B, Y_B, Z_B) of each structure are specified relative to the global coordinate system.

3) The input coordinate system (X_{inp}, Y_{inp}, Z_{inp}) of each input model included in a body is specified relative to the body coordinate system of that body.

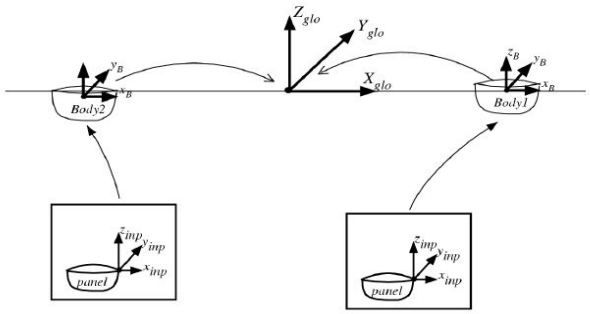

Fig. 1. Definition of multi-body coordinate system.

2.2 Surface waves

When first order potential theory are applied, the models may be exposed to planar and linear harmonic waves, i.e. waves described by the Airy wave theory. The incident waves may be specified by either wave lengths, wave angular frequencies or wave periods. The direction of the incident waves are specified by the angle between the positive x-axis and the propagating direction as shown in Fig. 2. The incident wave is defined as

$$\eta = Re\left[Ae^{i(\omega t - k(x\cos\beta + y\sin\beta))}\right] \tag{1}$$

which alternatively may be written as

$$\eta = A\cos(\omega t - k(x\cos\beta + y\sin\beta)) \tag{2}$$

where A is wave amplitude, β is direction of wave propagation, ω is wave angular frequency and k is absolute value of wave number. Equation (2) represents a wave with its crest at the origin for t=0 as shown in Fig. 2 (b).

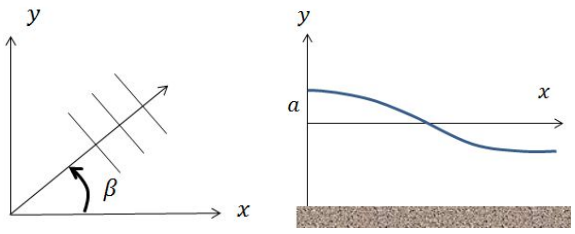

(a) (b)

Fig. 2. Definition of coordinates : (a) wave propagation direction and (b) wave phase at t=0.

2.3 Calculation of wave loads from potential theory

The potential theory is applied to calculate first order radiation and diffraction effects on large volume structures. The actual implementation is based on WAMIT (WaveAnalysisMIT) which uses a 3D panel method. WAMIT is a panel program designed to solve the boundary value problem for the interaction of water-waves. This implementation can be used for infinite and finite water depths and both single bodies and multiple interacting bodies can be analysed. The free surface condition is linearized for the first order potential theory while the non-linear free surface condition is imposed of the second order potential theory computation.

1) Boundary value problem formulation

The assumption of potential flow allows defining the velocity flow as the gradient of the velocity potential Φ that satisfies the Laplace equation

$$\nabla^2 \Phi = 0 \tag{3}$$

in the fluid domain. The harmonic time dependence allows defining a complex velocity potential ϕ, related to Φ by

$$\Phi = Re(\phi e^{i\omega t}) \tag{4}$$

where Re denotes the real part, ω is the frequency of the incident wave and t is time. The associated boundary value problem will be expressed in terms of the complex velocity potential ϕ, with the understanding that the product of all complex quantities with the factor $e^{i\omega t}$ applies. The linearized forms of the free-surface condition is

$$\phi_z - K\phi = 0 \ , \ z = 0 \tag{5}$$

where $K = \omega^2/g$ and g is the acceleration of gravity. The velocity potential of the incident wave is defined by

$$\phi_0 = \frac{igA}{\omega} \frac{\cosh(kz + H)}{\cosh kH} e^{-k(x\cos\beta + y\sin\beta)} \tag{6}$$

where the wave number k is the real root of the dispersion relation and β is the angle between the direction of propagation of the incident wave and the positive x-axis.

Linearization of the problem permits decomposition of the velocity potential into the radiation and diffraction components

$$\phi = \phi_R + \phi_D \tag{7}$$

$$\phi_R = i\omega \sum_{j=1,6} \xi_j \phi_j \tag{8}$$

$$\phi_D = \phi_0 + \phi_7 \tag{9}$$

The constants ξ_j denote the complex amplitudes of the body oscillatory motion in its six rigid-body degrees of freedom and ϕ_j means the corresponding unit-amplitude radiation potentials. The velocity potential ϕ_7 represents the scattered disturbance of the incident wave by the body fixed at its undisturbed position. The total diffraction potential ϕ_D denotes the sum of ϕ_7 and the incident wave potential.

On the undisturbed position of the body boundary, the radiation and diffraction potentials are subject to the conditions

$$\phi_{jn} = n_j \tag{10}$$

$$\phi_{Dn} = 0 \tag{11}$$

where $(n_1, n_2, n_3) = n$ and $(n_4, n_5, n_6) = r \times n$, $r = (x, y, z)$. The unit vector n is normal to the body boundary and points out of the fluid domain. The boundary value problem must be supplemented by a condition of outgoing waves applied to the velocity potential $\phi_j, j = 1,...,7$.

2.4 Interaction of multi-body

The boundary value problem of the multi-body interaction is explained. The diffraction potential for the isolated body can be defined by the incident potential.

$$\frac{\partial \phi_7^I}{\partial n} = -\frac{\partial \phi_0}{\partial n} \quad \text{on} \quad S_I \tag{12}$$

$$\frac{\partial \phi_7^{II}}{\partial n} = -\frac{\partial \phi_0}{\partial n} \quad \text{on} \quad S_{II} \tag{13}$$

where S_I and S_{II} denotes the wetted surface of the isolated body I and II respectively. ϕ_7^I and ϕ_7^{II} denotes the scattered potential to the isolated body I and II respectively. ϕ_0 is the incident wave potential of the isolated body. The radiation potential for the isolated body can be decomposed in the similar manner to the single body.

$$\phi_R^I = i\omega \sum_{j=1,6} \xi_j \phi_j^I \tag{14}$$

$$\phi_R^{II} = i\omega \sum_{j=1,6} \xi_j \phi_j^{II} \tag{15}$$

The radiation problem for the isolated body I and II can be given

$$\frac{\partial \phi_j^I}{\partial n} = n_j^I \quad \text{on } S_I \text{ (j = 1,2,...,6)} \tag{16}$$

$$\frac{\partial \phi_j^{II}}{\partial n} = n_j^{II} \quad \text{on } S_{II} \text{ (j = 1,2,...,6)} \tag{17}$$

where ϕ_j^I and ϕ_j^{II} denotes the decomposed radiation potential components for the isolated body I and II respectively and $n_j^{I,II}$ is a unit normal vector for the six degree of freedom for the isolated body I and II respectively. In equation (16) and (17), $n_j^{I,II}$ is given by

$$n_j^{I,II} = \begin{cases} (n_1, n_2, n_3)^{I,II} & \text{for } j = 1,2,3 \\ (n_4, n_5, n_6)^{I,II} = \breve{r} \times n & \text{for } j = 1,2,3 \end{cases} \tag{18}$$

where $\breve{r}$ denotes the relative distance from the origin to each body center.

The boundary value equation and the boundary condition for each body of the interaction problem are defined in the form of the radiation/scatter potential. The derivation of the formular is written

1) Radiation from I near II

(Body I is oscillating and body II fixed)

$$\frac{\partial \widehat{\phi_j^I}}{\partial n} = -\frac{\partial \phi_j^I}{\partial n} \quad \text{on } S_I \text{ (j = 1,2,...,7)} \tag{19}$$

$$\frac{\partial \widehat{\phi_j^I}}{\partial n} = 0 \quad \text{on } S_{II} \text{ (j = 1,2,...,7)} \tag{20}$$

2) Radiation from II near I

(Body II is oscillating and body I fixed)

$$\frac{\partial \widehat{\phi_j^{II}}}{\partial n} = -\frac{\partial \phi_j^{II}}{\partial n} \quad \text{on } S_{II} \text{ (j = 1,2,...,7)} \tag{21}$$

$$\frac{\partial \widehat{\phi_j^{II}}}{\partial n} = 0 \quad \text{on } S_I \text{ (j = 1,2,...,7)} \tag{22}$$

where $\widehat{\phi_j}^I$ denotes the interaction potential affected by radiation/scatter potential from the body I to the body II and $\widehat{\phi_j^{II}}$ is the potential by radiation/scatter potential from the body II to the body I. The potential when $j = 7$ means the scatter term (Kim, 2003).

Under the assumption that the responses are linear and harmonic, the twelve linear coupled differential equations of motion for two barges can be written as follows.

$$\sum_{j=1}^{12} \left[-\omega_e^2 (M_{ij} + A_{ij}) - i\omega_e B_{ij} + C_{ij} \right] \xi_j = F_i \text{ for=1,2,...12} \tag{23}$$

where M_{ij} is the generalized mass matrix for the barge1 and barge2, A_{ij} is the added mass coefficients, B_{ij} is the damping coefficients and C_{ij} is the restoring force matrix for barge1 and barge2, respectively, ξ_j is the complex amplitude of the response motion in each of the six degree of freedom for each body, and F_i is the complex amplitude of the wave exciting force for barge1 and barge2 (Kim and Ha, 2002).

3. Numerical analysis

3.1 Numerical model and configuration of two barges

Numerical simulations are conducted on the example barge with a jacket on top. The mesh and deck structure created by SESAM

GeniE can be seen in Fig. 3. There are three models needed during the calculation i.e. hydro model, mass model and structure model. Hydro model is used to calculate hydrodynamic forces on the structures and mass model is used to reports the imbalance condition between weight and buoyancy and used for solving equation of motion. WADAM (Wave Analysis by Diffraction and Morison Theory) is employed to calculate hydrodynamic loads on a structure model. WADAM is a general analysis program for calculation of wave-structure interaction for fixed and floating structures of arbitrary shape. The 3D potential theory in WADAM is based directly on the WAMIT program developed by Massachusetts Institute of Technology.

Main characteristics of model and mass data are given in Table 1. Direct input specification of a global mass matrix comprises giving the total mass of the structure together with the center of gravity and the gyration raddi.

In Fig. 4, two identical barges are placed floating side by side exposed to waves from different directions. Each of these barges is held in place by some moorings. The same FEM model will be used for both barges. RAOs (Response Amplitude Operators) of coupled barge1 (lee side), coupled barge2 (weather side) are compared to RAOs of single barge.

In order to investigate the effect of stiffness coupling, coupled stiffness matrix terms will be added to the system stiffness matrix. As shown in Table 2, we add a stiffness of 4 MN/m for all the springs to the multiple body modes in X-translation (surge) of barge 1, barge 2 and between two barges.

Table 3 shows the condition for the numerical calculation. Calculations of single barge and multiple barges are carried out for three wave directions (0°, 45°, 90°) and two water depths (300 m, 10 m). And 15 wave frequencies (0.2-1.6 rad/s) for each wave directions are chosen. The hull separation for side by side mooring are determined as 5 m, 10 m and 20 m.

Table 4 specifies the non-dimensionalized factors used in the results. The factor ρ denotes the density of the fluid, g is the acceleration of gravity, L is the characteristic length, V is the displaced volume of the body and A is the amplitude of the incoming waves. In Figs. 5-9, the abscissa axis means the angular frequency (rad/s) and ordinate values are amplitude. B1, B2, S are the abbreviations for barge1, barge2 and hull separation, respectively.

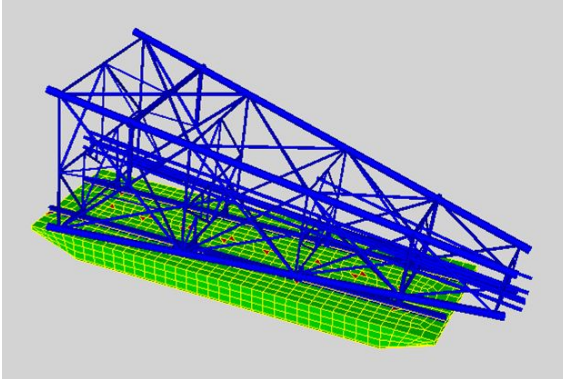

Fig. 3. The mesh and deck structure of barge model.

Table 1. Main dimensions of model and mass data

	Barge
Length (m)	91.44
Breadth (m)	27.43
Draft (m)	5.78
Displacement (m^3)	10304.6
Water plane area (m^2)	2486.99
Total mass (Kg)	1.00548E+007
Center of gravity X (m)	1.56904E-007
Center of gravity Y (m)	1.52257E-008
Center of gravity Z (m)	0.276799
Radius of gyration X	10.6455
Radius of gyration Y	26.574
Radius of gyration Z	27.1404
Number of nodes	3005
Number of beam segments	1191
Number of plates/shells	2266

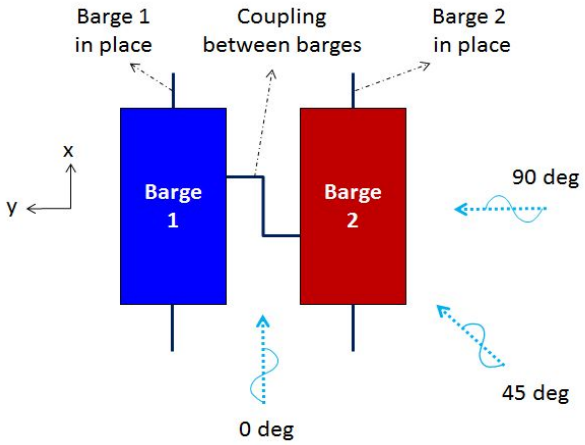

Fig. 4. Sketch of two moored barges with incident waves.

Table 2. Coupled stiffness matrix

Motion	X-translation of barge 1	X-translation of barge 2
surge	4E+006 (in place)	-4E+006 (coupling)
	-4E+006 (coupling)	4E+006 (in place)

Table 3. Conditions for the numerical simulation

case	Wave Direction	Angular Frequency	Depth [m]	Hull Separation [m]
1	0 45 90	0.2rad/s-1.6rad/s	300	5
2				10
3				20
4			10	5
5				10
6				20

Table 4. Non-dimensionalising factors for matrices

	$entry_{ij}$	$mode_i$	$mode_j$
	i=1-3, j=1-3	i=1-3	j=4-6
Added mass	ρV		
Damping	$\rho V\sqrt{(g/L)}$		
Exciting force		$\rho VgA/L$	ρVgA
Motion		A	A/L

3.2 Added mass, potential damping and exciting force in sway motion

In Fig. 5 (a), hydrodynamic interaction is significant in added mass and potential damping due to sway motion between 0.8-1.0 rad/s. This resonance phenomena are similar to the numerical results by Hong et al. (2005) depicting interaction effect around 0.8 rad/s in heave motion of side by side moored vessels. As previously presented by some papers, sway exciting force of lee side barge is smaller than those of weather side barge with transverse waves as shown in Figs. 5 (b) and (c). However, the lee side barges get sharp peak between 0.8-1.3 rad/s depending on hull separation. The sheltering effect of the barges is not shown at 1.3 rad/s with hull separation 20 m. Sway exciting forces are influenced by hull separation in these mooring condition unlike the cases of no mooring condition by Ali and Inoue (2005).

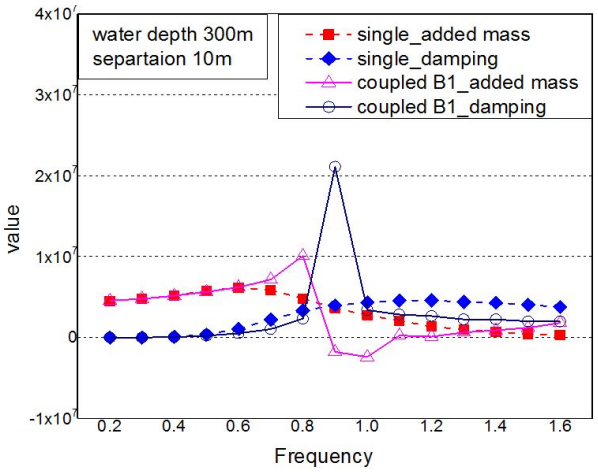

(a) added mass and damping in sway motion

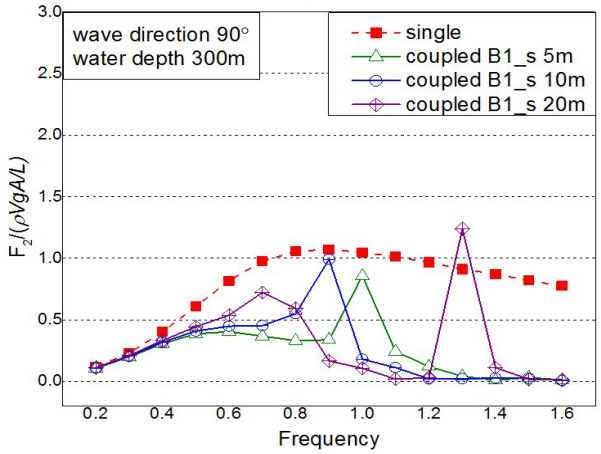

(b) sway force of lee side

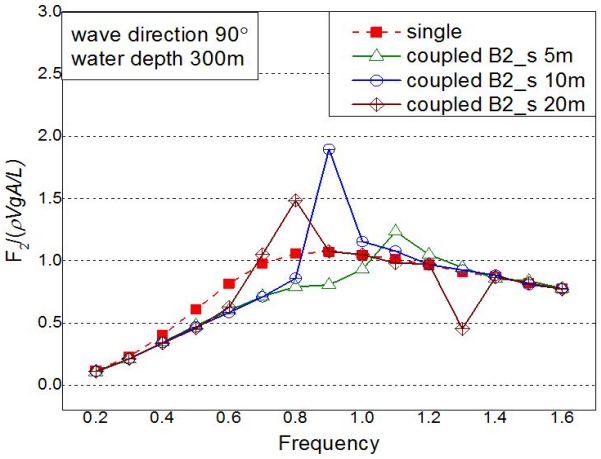

(c) sway force of weather side

Fig. 5. Added mass, potential damping and exciting force.

3.3 Motion response analysis

The results are classified by incident waves (0°, 45°, 90°) and motion responses are described from an angle of separation effect.

When the barge receive the wave from longitudinal direction, the effect of hull separation can be seen in sway, heave and roll motion. In Figs. 6 (a) and (b), the peaks for sway and heave motion occurred at higher frequencies as hull separation decreased. In Figs. 6 (b) and (c), the magnitude of peaks in heave and roll motion tends to decrease as hull separation decreases in the range of 0.9-1.3 rad/s. In Fig. 6 (c), lee side coupled barge produces two peaks in each of hull separations unlike the case of single barge in roll motion.

However, the difference cannot be seen between hull separation both sway and heave motion with transverse waves as shown in Fig. 7. Compared with single barge, response magnitudes of coupled lee side barge are reduced between 0.9-1.6 rad/s in sway and heave motion. In Figs. 7 (c), slight fluctuation of heave is observed at 1.0 rad/s with hull separation of 20 m.

The motion responses are less affected by hull separations with transverse and oblique waves. We therefore depicted the respective motion of coupled two barges with oblique waves with hull separation 10 m. Xu and Dong (2013) described the pitch is not highly affected by hydrodynamic interactions except the resonance region of captive ship model and some region of semi-captive ship model with forward speed. In this Fig. 8, roll and pitch of barge 1 and barge 2 without forward speed show discrepancy in amplitude between 0.7-1.2 rad/s whereas the responses of heave are much the same between single and each of the coupled barges. On the whole, mooring conditions arranging the barges in place are thought to affect hydrodynamic interactions.

3.4 Water depth effect

When the barge place at the shallow water depth (10 m), several features of lee side barge can be seen as follows in comparison with the cases of deep water depth (300 m). Compared with Fig. 5 (b), the sharp peak at 1.3 rad/s of hull separation 20 m disappear in Fig. 9 (a). As shown in Fig. 9 (a), the peaks for sway force are situated at higher frequencies as hull separation narrowed with transverse waves.

In Figs. 9 (b) and (c), we compared the results of depths 300 m and 10 m for sway force and sway motion of lee side barge by changing wave directions. According to Fig. 9 (b), the peaks for sway force with water depth of 10 m are situated at lower frequencies compared to the depth of 300 m, even when incident

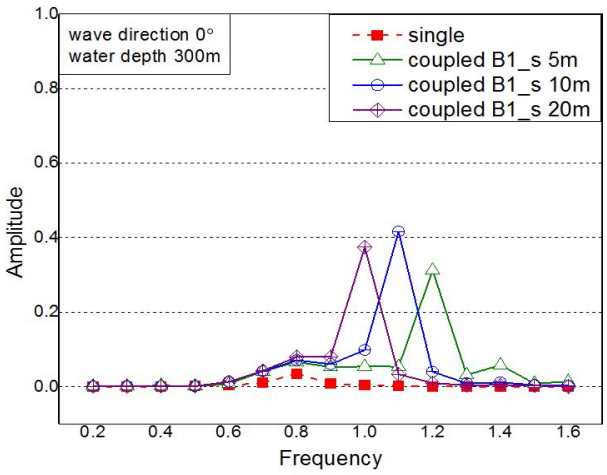

(a) sway (lee side)

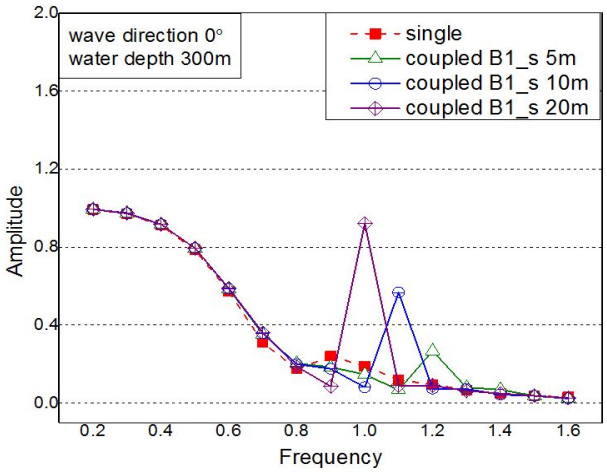

(b) heave (lee side)

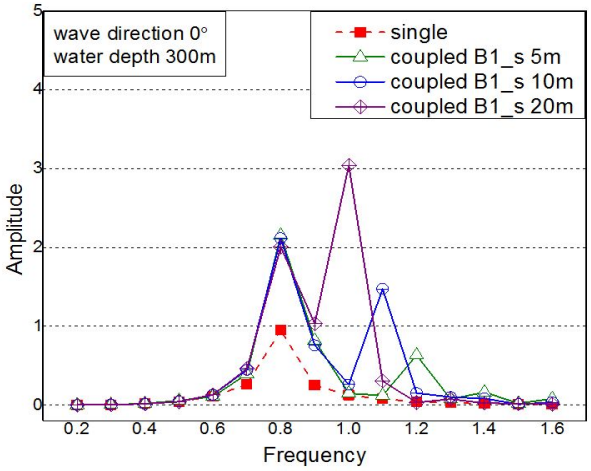

(c) roll (lee side)

Fig. 6. Comparison of responses with longitudinal waves.

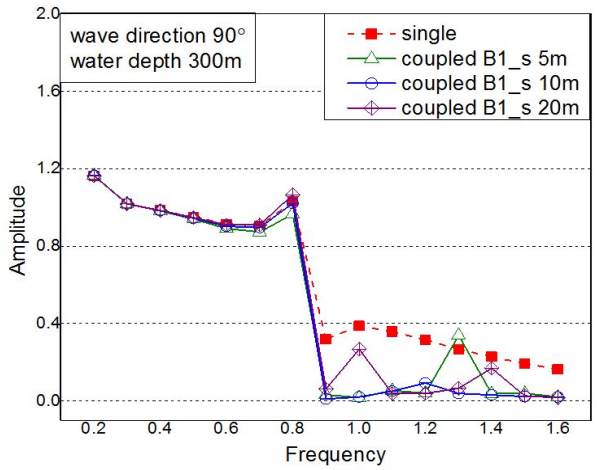

(a) sway (lee side)

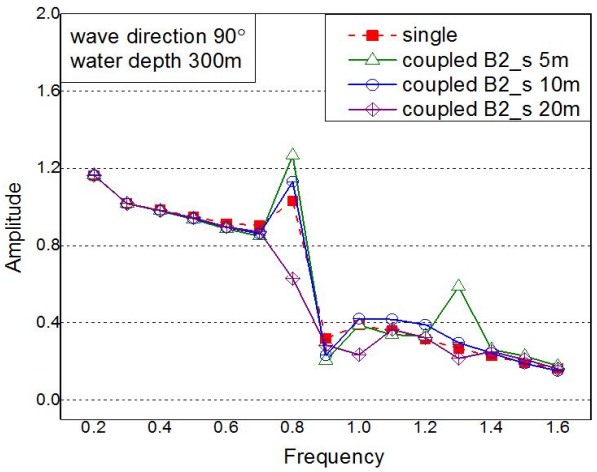

(b) sway (weather side)

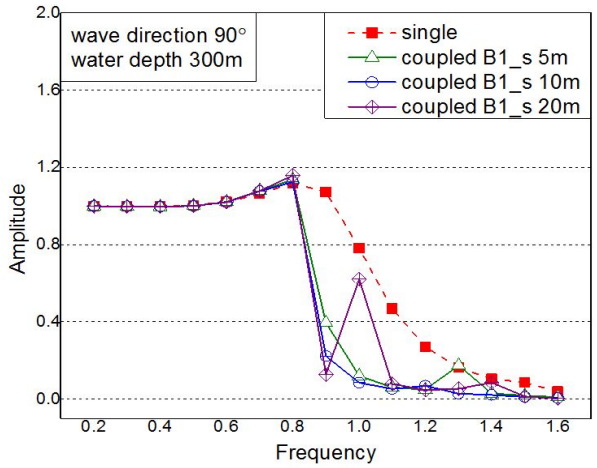

(c) heave (lee side)

Fig. 7. Comparison of responses with transverse waves.

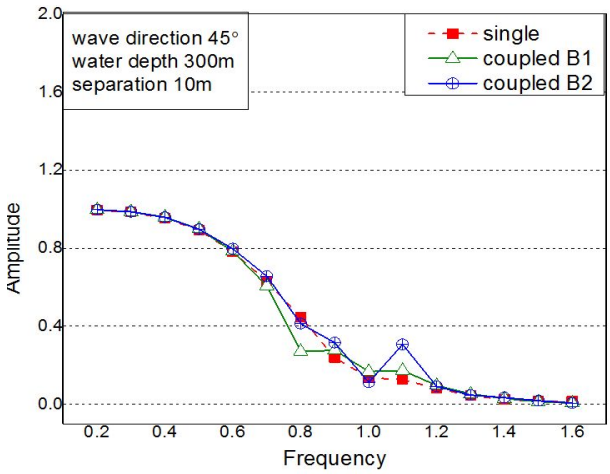

(a) heave

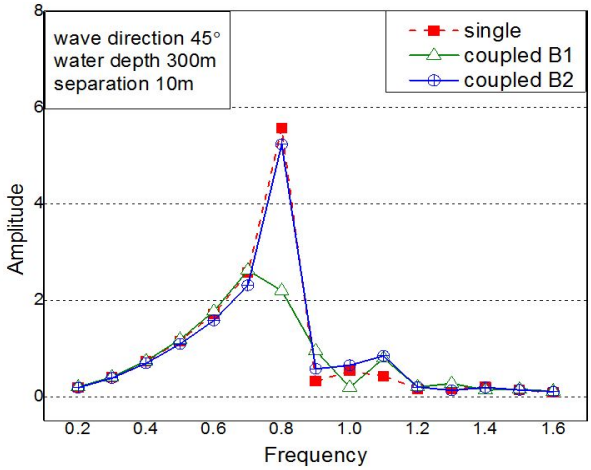

(b) roll

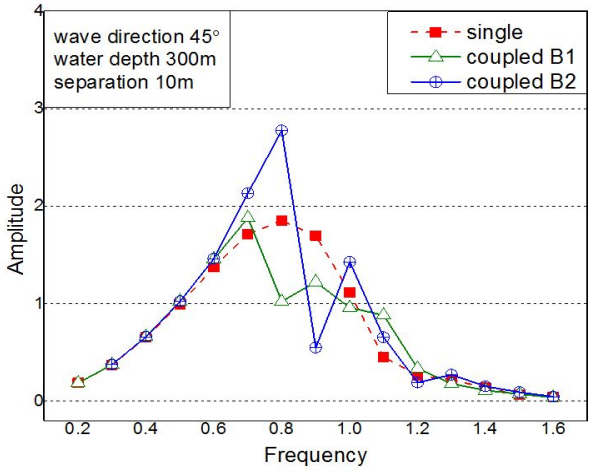

(c) pitch

Fig. 8. Comparison of responses with oblique waves.

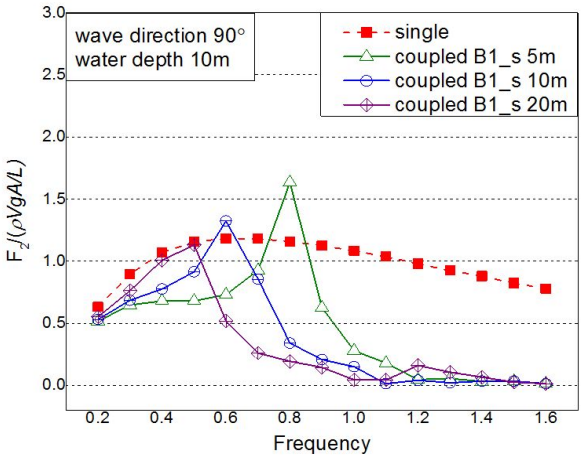

(a) sway force (lee side)

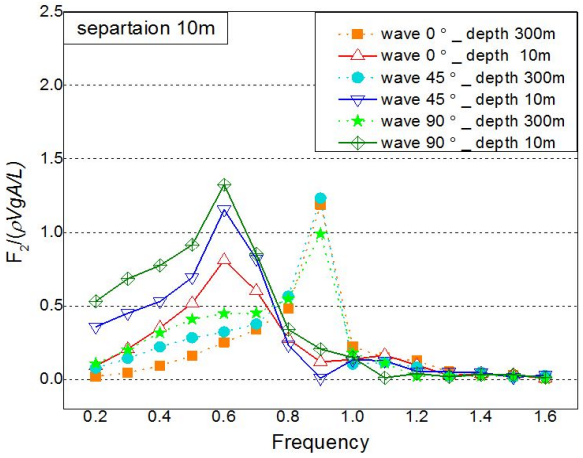

(b) sway force (lee side)

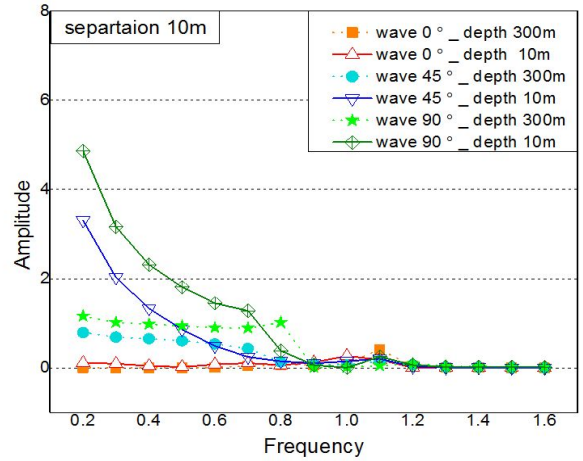

(c) sway motion (lee side)

Fig. 9. Comparison of water depth effect

waves change. Given a depth of 10 m in Fig. 9 (c), sway motions on the lee side barge make a significant difference between 0.2-0.8 rad/s with longitudinal waves.

4. Conclusion

Two rectangular barges in close proximity were simulated to analyze the characteristics of motion responses due to hydrodynamic interactions. Influencing factors such as wave direction, hull separation and water depth are considered.

(1) In case of deep water depth, the sheltering effect of lee side barge is not shown at certain frequency with hull separation 20 m in transverse waves. This phenomenon disappear at the shallow water depth.

(2) Regarding motion responses, the separation effect between the barges is more clear with longitudinal waves and a shallow water depth. However, sway forces are influenced by hull separation with transverse waves. The mooring condition arranging the barges in place affects hydrodynamic interactions.

(3) The peaks for sway and heave motion and sway force occurred higher frequencies as hull separation narrowed with longitudinal and transverse waves.

(4) Given a depth of 10 m, the sway motion on the lee side of a coupled barge stands out with transverse and oblique waves. Also, the peaks for sway force are situated at the lower frequencies even the incident wave changes.

In this study, we investigated hydrodynamic interactions between two moored barges with regular waves. In order to apply to actual sea states, RMS heave and pitch motion of moving barges should also be taken into account together with added resistance according to the Beaufort scale. Therefore, further research is strongly needed to extend the ships involving forward speed under the actual sea circumstances for the intensive study of ship to ship interaction.

References

[1] Ali, M. T. and Y. Inoue(2005), On Hydrodynamic Interaction between Two Rectangular Barges Floating Side-by-Side in Regular Waves, Proceedings of the International Conference on Mechanical Engineering, Dhaka, Bangladesh, pp. 1-6.

[2] Buchner, B., A. Dijk and J. Wilde(2001), Numerical Multiple-Body Simulations of Side-by-Side Mooring to an FPSO, Proceedings of 11th International Offshore and Polar Engineering, Stavanger, Norway, pp. 1-11.

[3] Bunnik, T., W. Pauw and A. Voogt(2009), Hydrodynamic Analysis for Side-by-Side Offloading, Proceedings of the 19th International Offshore and Polar Engineering Conference, Osaka, Japan, pp. 648-653.

[4] Choi, Y. R. and S. Y. Hong(2002), An Analysis of Hydrodynamic Interaction of Floating Multi-body using Higher-Order Boundary Element Method, Proceedings of 12th International Offshore and Polar Engineering Conference, Kitakyushu, Japan, pp. 303-308.

[5] Clauss, G. F., M. Dudek and D. Testa(2013), Gap Effects at Side-by-Side LNG-transfer Operations, Proceedings of the 32nd International Conference on Ocean, Offshore and Arctic Engineering, Nantes, France, pp. 1-8.

[6] DNV(2010a), Global Performance Analysis of Deepwater Floating Structures, Recommended Practice, DNV-RP-F205, Det Norske Veritas, Hovik, Norway, pp. 7-8.

[7] DNV(2010b), Wave Analysis by Diffraction and Morison theory, Report No. 94-7100, Det Norske Veritas, Hovik, Norway, pp. 35-65.

[8] Fournier, J. R., M. Naciri and X. B. Chen(2006), Hydrodynamics of Two Side-by-Side Vessels Experiments and Numerical Simulations, Proceedings of the 16th International Offshore and Polar Engineering Conference, San Francisco, USA, pp. 158-165.

[9] Hong, S. Y., J. H. Kim, S. K. Cho, Y. R. Choi and Y. S. Kim(2005), Numerical and Experimental Study on Hydrodynamic Interaction of Side-by-Side Moored Multiple Vessels, Ocean Engineering, Vol. 32, pp. 783-801.

[10] Kim, K. H. and Y. H. Kim(2008), Time-Domain Analysis on Motion Responses of Adjacent Multiple-Bodies in Waves, Journal of the Society of Naval Architects of Korea, Vol. 45, No. 1, pp. 63-72.

[11] Kim, M. S. and M. K. Ha(2002), Prediction of Motion Responses between Two Offshore Floating Structures in Waves, Journal of Ship & Ocean Technology, Vol. 6, No. 3, pp. 13-25.

[12] Kim, Y. B.(2003), Dynamic Analysis of Multiple-Body Floating Platforms Coupled with Mooring Lines and Risers, Ph. D. Thesis, Texas A&M university, pp. 28-40.

[13] Pessoa, J., N. Fonseca and C. G. Soares(2015), Numerical Study of the Coupled Motion Responses in Waves of Side-by-Side LNG Floating Systems, Applied Ocean Research, Vol. 51, pp. 350-366.

[14] Xu, Y. and W. Dong(2013), Numerical Study on Wave Loads and Motions of Two Ships Advancing in Waves by using Three-Dimensional Translating-pulsating Source, The Journal of Acta Mechanica Sinica, Vol. 29, No. 4, pp. 494-502.

Received : 2016. 08. 10.
Revised : 2016. 09. 07. (1st)
: 2016. 10. 18. (2nd)
Accepted : 2016. 10. 27.